Journal of the Optical Society of Korea
Vol. 19, No. 1, February 2015, pp. 29-37

ISSN: 1226-4776(Print) / ISSN: 2093-6885(Online)
DOI: http://dx.doi.org/10.3807/JOSK.2015.19.1.029

Image-Quality Enhancement for a Holographic Wavefront Color Printer by Adaptive SLM Partitioning

Sunghee Hong[1], Elena Stoykova[2,3], Hoonjong Kang[2*], Youngmin Kim[2], Jisoo Hong[2], Joosup Park[2], and Kiheon Park[1]

[1]*School of Electronic and Electrical Engineering, Sung Kyun Kwan University, 2066 Seobu-ro, Jangan-gu, Suwon 440-746, Korea*
[2]*Realistic Media Platform Research Center, Korea Electronics Technology Institute, 8 Floor, #1599, Sangam-dong, Mapo-gu, Seoul 121-835, Korea*
[3]*Institute of Optical Materials and Technologies, Acad. G. Bonchev Str., Bl. 109, 1113 Sofia, Bulgaria*

(Received December 4, 2014 : revised January 7, 2015 : accepted January 12, 2015)

The wavefront printer records a volume-reflection hologram as a two-dimensional array of elemental holograms from computer-generated holograms (CGHs) displayed on a spatial light modulator (SLM). The wavefront coming from the object is extracted by filtering in the spatial-frequency domain. This paper presents a method to improve color reproduction in a wavefront printer with spatial division of exposures at primary colors, by adaptive partitioning of the SLM in accordance with the color content encoded in the input CGHs, and by the controllable change of exposure times for the recording of primary colors. The method is verified with a color wavefront printer with demagnification of the object beam. The quality of reconstruction achieved by the proposed method proves its efficiency in eliminating the stripe artifacts that are superimposed on reconstructed images in conventional mosaic recording.

Keywords : Wavefront printer, SLM, Volume hologram, Color recording
OCIS codes : (090.1705) Color holography; (090.1760) Computer holography; (230.6120) Spatial light modulators

I. INTRODUCTION

The formulation of the holographic principle by Dennis Gabor in 1948 [1], and the invention of lasers a decade later, laid the foundations of holographic technology. The introduction of carrier frequency in holographic recording by Leith and Upatnieks in 1962 [2], and the publication by Denisuyk [3] in the same year on recording white-light-viewable reflection holograms, pushed forward optical metrology and display holography of three-dimensional (3D) still images. Advances in computers and optoelectronics enabled the development of holographic imaging technologies, such as holographic video [4] and holographic printing [5]. The current status of research on dynamic holographic display indicates that this technology still has a long way to go before the release of a commercial product. By comparison, the technology for holographic printing of 3D still images is the one closest to commercialization. Holographic stereogram printers, also known as direct-write digital holographic printers, have been developed and released as commercial products by Geola, Ultimate, and Zebra [6]. These printers rely on a holographic stereogram method, which records parallax-related images displayed on a spatial light modulator (SLM) onto a holographic emulsion as a volume reflection hologram [6-8]. The input data formed from incoherently acquired perspective images of the 3D scene carry only directional information, and thus this printing method inevitably suffers from longitudinal distortion in the reconstruction of deep scenes. In contrast, the recently proposed holographic fringe and wavefront printers use as input data for the SLM a computer generated hologram (CGH) [9-14], which encodes both directional and depth information. In the fringe printer the CGH is directly transferred onto the holographic emulsion, without a reference beam during recording [9]. The output is a thin transmission hologram that lacks color selectivity. The output of the wavefront printer, on the other hand, is

*Corresponding author: hoonjongkang@keti.re.kr
Color versions of one or more of the figures in this paper are available online.

a volume reflection hologram. This method relies on extraction of the wavefront coming from the 3D object, and thus resembles an analog holography recording process [10-14]. The main advantage of this method is distortion-free color reconstruction of target objects from the printed hologram, but it requires a 3D object model and a vast amount of calculations to generate the fringe pattern. The latter problem has been actively addressed lately by elaborating approaches for fast generation of CGHs. In addition, as the performance of multicore CPUs and GPUs improves, the problem of accelerated CGH computation can be solved.

Whilst commercialization of holographic printers and the wavefront printer in particular is forging ahead, a lot of problems should still be solved to elicit a positive public response. Shortcomings such as the small viewing angle provided by the printed hologram, unfavorable lighting conditions, and degradation of image quality when printing in color, presently prevent holographic printers from satisfying the demands of the market. A wider viewing angle could be obtained by improving the optical performance of the holographic printer. The fundamental requirement of holographic technology for coherent illumination renders impossible the use of regular lighting, such as fluorescent light or distributed light sources, and specialized lighting solutions should be developed. Research has been performed on the reproducibility of colors in color printing, but not much has been done on finding methods to improve image quality in the process of color production [15-17].

One prospective approach is mosaic recording [17], with spatial division of exposures in primary colors. It can be applied to both holographic stereogram and wavefront printing, due to spatial multiplexing of the printed hologram via sequential exposure of a large number of elemental holograms. In mosaic recording a single elemental hologram carries only one of the primary colors, and hence a crucial issue is to guarantee its small size. This type of recording corresponds to single-exposure recording, and produces bright reconstruction in saturated colors; however, it is vulnerable to the occurrence of artifacts superimposed on the reconstructed image that lead to quality degradation.

The aim of this paper is to propose a method to reduce image-quality degradation in a color wavefront printer with spatial division of exposures in primary colors. Image-quality improvement relies on the wavefront printing principle, which allows for rearrangement of input information. The paper is structured as follows: In Sec. 2 we briefly explain the principle of wavefront printing by presenting the optical design of our printing system, and describe the situation in which recording of a color mosaic worsens image quality. In Sec. 3 we show how to determine the color content to be encoded in a current CGH, and present the method for accelerated CGH computation that is used in the paper. In Sec. 4 we propose our method for improving color reproduction, by adaptive spatial partitioning of the SLM and controlling the exposure times at delivery of primary colors to the holographic emulsion. Experimental verification of the method is given in the final Sec. 5.

II. COLOR DEGRADATION IN MOSAIC RECORDING

Holographic printers print holograms from digital contents onto a holographic plate. The printer input is a two-dimensional (2D) array of elemental digital patterns that encode the light field coming from the 3D object to multiple viewpoints. Accordingly, the printer output is an analog hologram composed of a large number of individually recorded elemental holograms. The digital contents to be recorded in an elemental hologram are displayed on an SLM as a 2D array of real numbers. The light diffracted from the SLM is optically processed and directed to the holographic plate. The output hologram is recorded successively by updating the information on the SLM and shifting the holographic plate with an X-Y stage. The digital input and types of recording for existing holographic printers are given in Table 1. As can be seen, the holographic stereogram printer and the wavefront printer with amplitude-type CGH easily support color printing of white-light-viewable holograms.

In the wavefront printer that we recently proposed [12], the light wavefront to be recorded is extracted from an amplitude-type CGH $H(\xi,\ \eta)$:

$$H(\xi,\eta)=|O(\xi,\eta)+R(\xi,\eta)|^2=OO^*+RR^*+OR^*+O^*R \qquad (1)$$

where ξ and η are coordinates at the plane of the SLM, $O(\xi,\ \eta)$ is the beam coming from the object, and the digital reference wave $R(\xi,\ \eta)$ for computation of the CGH is slightly inclined at an angle θ with respect to the normal to the SLM plane. The object beam is extracted by illuminating the SLM with a plane wave that impinges normally upon its surface. The light diffracted from the SLM contains the zeroth-order beam OO^*+RR^*, which is directed along the optical axis, and the ±1 -order beams OR^* and O^*R, which propagate at an angle $\pm\theta$ with respect

TABLE 1. Types of holographic printers

Printer type	Digital input	Reference wave	Output hologram
Holographic stereogram printer	Parallax related images	Yes	Reflection volume-type
Direct fringe printer	CGH (amplitude)	No	Thin transmission
Wavefront printer	CGH (amplitude or phase)	Yes	Reflection volume-type

to this axis. The beams OR^* and O^*R focus at a distance from the hologram on its opposite sides, to form the virtual image and the real image. These beams are collected by a lens whose rear focal plane corresponds to the spatial-frequency domain, where the Fourier spectrum $F\{H(\xi, \eta)\}$ of the hologram (with F denoting the Fourier transform) consists of three spatially separated terms, $F\{OO^* + RR^*\}$, $F\{OR^*\}$, and $F\{O^*R\}$ respectively. A spatial filter is located at the rear focal plane of the lens and is shifted with respect to the optical axis to transmit only the term $F\{OR^*\}$, which carries the light coming from the object.

In the optical design of our wavefront printer, the spatial filter is located at the rear focal plane of lens L_1 with focal distance f_1 and the front focal plane of lens L_2 with focal distance $f_2 << f_1$. The lens L_2 reconstructs a demagnified version of the beam OR^* at demagnification ratio $M = f_2 / f_1$. Contrary to the holographic stereogram printer [8], demagnification of the elemental hologram for a wavefront printer is not imposed by the means of encoding the 3D content onto the holographic plate. The elemental hologram in the wavefront printer is a part of a hologram that could be as large as the active area of the SLM. Demagnification is performed to avoid grid artifacts due to imperfections of the optical recording scheme, and to allow for mosaic delivery of exposures in primary colors.

Basically, color production in a holographic printer is accomplished with a combination of red (R), green (G), and blue (B) lasers. A color hologram can be recorded by a multiple-exposure method that forms each elemental hologram as a combination of three color channels [6, 18]. The drawback of this approach is worsening of color reproduction, due to crosstalk between the RGB channels, and decrease in the light-sensitive material's dynamic range attributed to each color. Thus the space-division exposure method is preferable for holographic printers. This method resembles the formation of color pixels in LCD displays, with one significant difference: A single pixel in an LCD display (Fig. 2(a)) carries three colors and has a size well below the threshold of human visual acuity. This plus a large number of pixels guarantee that the spatial separation of primary colors in an LCD display remains unnoticeable to the viewer. However, color production by mosaic delivery in a holographic printer receives one color per elemental hologram, as depicted in Fig. 2(b) [16]. If the color red is dominant in the content to be printed, the elemental holograms corresponding to the green and blue color channels are repeatedly printed as low-intensity patterns, and the color they reconstruct will be almost black. The color channels that are practically empty create a regular dark pattern, i.e. a stripe pattern is formed. Such a stripe pattern can be observed in Fig. 3, which shows reconstruction from a hologram printed with the wavefront printing system described in Sec. 5, using conventional mosaic recording. A similar pattern can be also found in Ref. [16]. Repetition of low-intensity recording has a damaging effect on the overall resolution, and becomes more pronounced if the size of the image decreases.

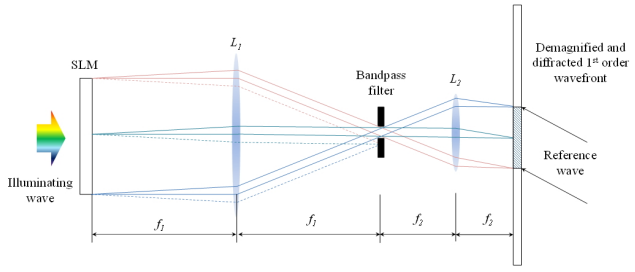

FIG. 1. Design of the optical head of a wavefront printer with an amplitude type SLM and demagnification of the filtered first-order wavefront.

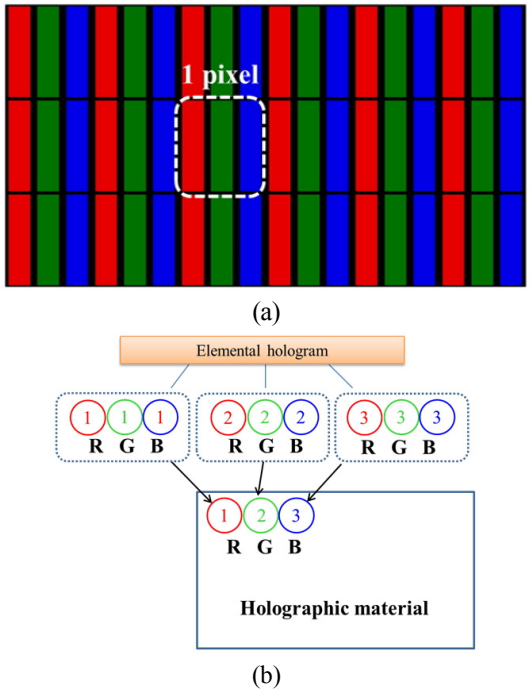

FIG. 2. (a) Formation of color pixels in an LCD display. (b) Holographic printing by mosaic delivery of exposures in primary colors.

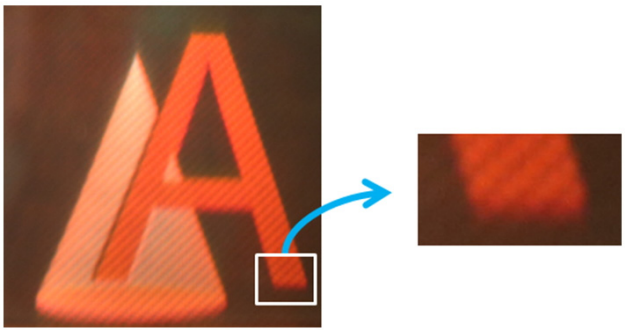

FIG. 3. Striped structure superimposed on an image reconstructed from a hologram and printed by a wavefront printer with mosaic recording.

III. DETERMINATION OF THE COLOR CONTENT

The degree of color degradation in mosaic recording depends on the color content to be encoded into elemental holograms. Spatial multiplexing applied in holographic printing closely resembles the ray-casting approach, which is now gaining popularity for CGH computation. A ray-casting algorithm divides the hologram plane into subholograms and casts rays from each subhologram onto the objects in the 3D scene [19, 20]. The objects are populated with primitives such as points or polygons, and appropriate methods (such as summation of spherical waves [19, 20] or angular spectrum propagation [21]) can be applied to describe the light wavefront coming from the primitives to the plane of the hologram. In this paper we adopt the ray-casting approach to generate the 3D content by using point-cloud object representation, in the scheme of Fig. 4. A set of point clouds was extracted for all elemental holograms, and fringe patterns were computed for each of them using the corresponding point clouds.Suppose that the hologram plane is divided into $K \times L$ elemental holograms. The object data in the point cloud seen from the elemental hologram $H^{ij}(x, y)$, where indices $i = 1, \ldots K$ and $j = 1, \ldots, L$ show its location at the hologram plane, consist of P^{ij} point sources with 3D coordinates $(x_p^{ij}, y_p^{ij}, z_p^{ij})$, $p = 1, 2, \ldots, P^{ij}$, which emit spherical waves with RGB amplitudes $(r_p^{ij}, g_p^{ij}, b_p^{ij})$, $p = 1, 2, \ldots, P^{ij}$ and phases (φ_p^{ij}), $p = 1, 2, \ldots, P^{ij}$. The color content for this elemental hologram is determined from

$$R^{ij} = \sum_{p=1}^{P^{ij}} r_p^{ij} \quad , \qquad G^{ij} = \sum_{p=1}^{P^{ij}} g_p^{ij} \quad , \qquad B^{ij} = \sum_{p=1}^{P^{ij}} b_p^{ij} \tag{2}$$

The ray-casting approach is highly suitable for incorporating effects that create photorealistic imaging, such as viewpoint-dependent occlusion, shadowing, reflection, etc. Some of

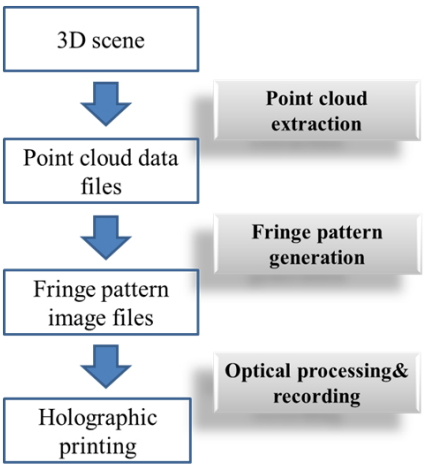

FIG. 4. Generation of 3D content for wavefront holographic printing.

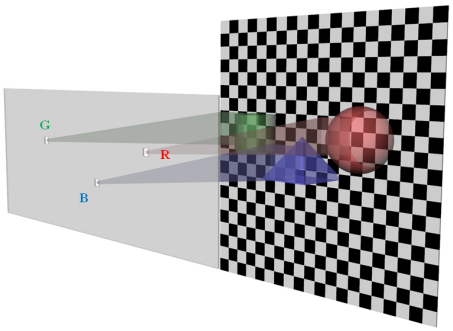

FIG. 5. Computation of CGHs to be recorded into elemental holograms by the ray-casting approach.

these effects are encoded in the phases (φ_p^{ij}), $p = 1, 2, \ldots, P^{ij}$, others in the amplitudes of the primary colors $(r_p^{ij}, g_p^{ij}, b_p^{ij})$, $p = 1, 2, \ldots, P^{ij}$. In view of the limit on the maximum viewing angle, set by the SLM pixel pitch and visual effects such as occlusion, reflection, etc., the point clouds and hence the color content may vary with the location of the elemental hologram, as depicted in Fig. 5. The elemental holograms in Fig. 5 receive input from three different point clouds with dominant red, green, and blue components in the overall color content. Therefore, for the hologram in Fig. 5, mosaic recording by encoding primary colors into separate elemental holograms may worsen color reproduction.

Calculation of $H^{ij}(x, y)$ for P^{ij} point sources for a reference plane wave by following the Rayleigh-Sommerfeld (R-S) diffraction model requires evaluation of the object beams at primary wavelegths:

$$O_q^{ij}(\xi,\eta) = \sum_{p=1}^{P^{ij}} \frac{a_p^{ij}}{d_p^{ij}} \exp\left(j\varphi_p^{ij}\right) \exp\left(jk_q d_p^{ij}\right),$$
$$a_p^{ij} \equiv r_p^{ij}, g_p^{ij}, b_p^{ij}, p = 1, \ldots, P^{ij}, q = r, g, b \tag{3}$$

where $d_p^{ij} = \sqrt{\left(\xi - x_p^{ij}\right)^2 + \left(\eta - y_p^{ij}\right)^2 + \left(z_p^{ij}\right)^2}$ is the distance between the point source at $(x_p^{ij}, y_p^{ij}, z_p^{ij})$ and the point on the CGH, r_p^{ij}, g_p^{ij}, b_p^{ij} are the amplitudes of the light field emanated by this source at the primary wavelengths λ_q, $q = r, g, b$ (where the index q indicates which primary color is chosen), and $k_q = 2\pi/\lambda_q$ is the wave number. In our wavefront printer we employ a high-resolution SLM with 1920 × 1080 pixels for display of the CGHs, which increases the computational burden, since Eq. (3) must be computed for each pixel. For this reason, we develop and apply a method to accelerate the computation, based on phase-added stereogram approaches [22-23]. According to this method, the elemental hologram in the hologram plane (ξ, η) is divided into $M \times N$ square segments of size $Q \times Q$ pixels each. The numerical model of the CGH in each segment is expressed as

$$H_{mn}^{ij,q}(\xi,\eta) = F^{-1}\left\{I_{mn}^{ij,q}(u,v)\right\}, \tag{4}$$

$$I_{mn}^{ij,q}(u,v) = \sum_{p=1}^{P^{ij}} \frac{a_p^{ij,q}}{d_{pmn}^{ij}} \exp\left[j\left(k_q d_{pmn}^{ij} + \varphi_p^{ij}\right)\right] \exp\left\{j2\pi\left[u_{pmn}^{ij,q}\left(\xi_{cmn}^{ij} - x_p^{ij}\right) + v_{pmn}^{ij,q}\left(\eta_{cmn}^{ij} - y_p^{ij}\right)\right]\right\} \times \delta\left(u - u_{pmn}^{ij,q}, v - v_{pmn}^{ij,q}\right), \quad (5)$$

where $H_{mn}^{i,j,q}(\xi, \eta)$ is the holographic fringe pattern calculated at a primary color q in the mn-th segment of the ij-th elemental hologram, and $I_{mn}^{i,j,q}(u, v)$ is its distribution in the spatial-frequency domain. The distance d_{pmn}^{ij} is determined with respect to the segment's central point $(\xi_{cmn}^{ij}, \eta_{cmn}^{ij})$. And the spatial frequencies u_{pmn}^{ij} and $v_{pmn}^{ij,q}$ are given by

$$u_{pmn}^{ij,q} = \lambda_q^{-1}\left(\sin\theta_{\xi pmn}^{ij} - \sin\theta_{\xi r}\right), \quad (6)$$

$$v_{pmn}^{ij,q} = \lambda_q^{-1}\left(\sin\theta_{\eta pmn}^{ij} - \sin\theta_{\eta r}\right), \quad (7)$$

where $\theta_{\xi pmn}^{i,j}$ and $\theta_{\eta pmn}^{i,j}$ are the incidence angles from the p-th object point in the point cloud p = 1, 2, ..., P^{ij} to the central point of the mn-th segment, and $\theta_{\xi r}$ and $\theta_{\eta r}$ are the illumination angles of the plane reference wave $R(\xi, \eta) = \exp\{jk(\xi\sin\theta_{\xi r} + \eta\sin\theta_{\eta r})$ with respect to the ξ and η axes. The segment size is determined by the requirement to provide quality of reconstruction close to that observed for a CGH computed by the R-S model. We apply fast Fourier transform in Eq. (4), with zero-padding for a number of pixels larger than $Q \times Q$, to decrease the error due to discretization of the spatial frequencies.

We conduct a numerical experiment, in which the object is a point at some distance from the hologram plane. The simulated hologram encodes the object beam as a fringe pattern, varying from 0 to 255 levels of intensity, for a reference wave that is normal to the plane of the hologram. The size of the hologram is 1024 × 1024 pixels, and the wavelength is 532 nm. To illustrate worsening of reconstruction when one or two color channels are practically empty, we convolute the hologram with a stripe pattern of zero intensity. We vary the width of the stripes to cover 25%, 50%, or 75% of the whole hologram. The obtained holograms are shown in Fig. 6. We also plot in Fig. 6 the cross sections of the reconstructions along a line passing through the point object and normal to the stripes. Degradation in the quality of reconstruction is clearly seen; as should be expected, it expresses itself as a strong decrease in intensity with occurrence of subsidiary peaks.

We also objectively assess the quality of images reconstructed from the holograms with stripes by using the peak signal-to-noise ratio (PSNR). This metric estimates globally the similarity between two images by calculating the PSNR as follows

$$\mathrm{PSNR} = 10\log_{10}\left(\frac{\mathrm{MAX}_I}{\mathrm{MSE}}\right)^2 = 20\log_{10}\left(\frac{\mathrm{MAX}_I}{\mathrm{MSE}}\right) \quad (8)$$

$$\mathrm{MSE} = \frac{1}{IJ}\sum_{i=0}^{I}\sum_{j=0}^{J}\left|f_{ij} - g_{ij}\right|^2 \quad (9)$$

where $\mathrm{MAX_I}$ is the dynamic range of the pixel values (255 for 8-bit grayscale images), f_{ij}, i = 1, ..., K, j = 1, ..., L is the value of the undistorted image obtained without stripes at a pixel (i, j), g_{ij}, i = 1, ..., K, j = 1, ..., L is the values of

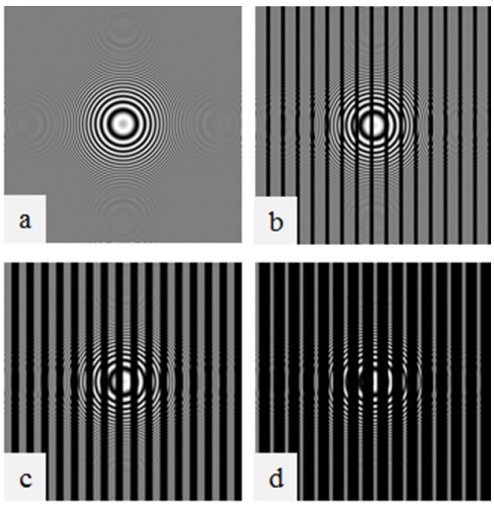

(A)

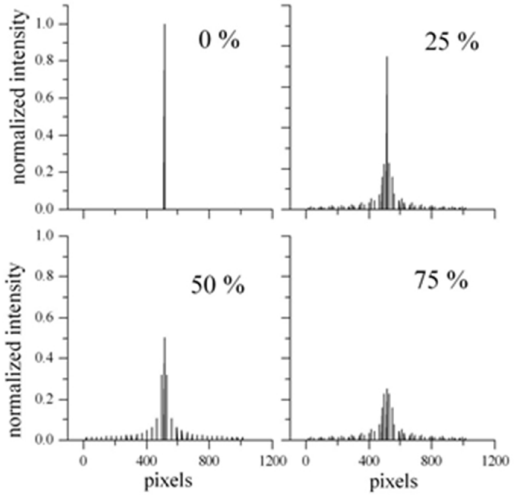

(B)

FIG. 6. (A) A grayscale, single-point CGH superimposed with a pattern of black stripes; the stripes occupy (a) 0%, (b) 25%, (c) 50%, or (d) 75% of the hologram. (B) Cross sections of reconstructions corresponding to (a), (b), (c), and (d) along a line that passes through the point object and which is normal to the stripes.

TABLE 2. PSNR of reconstructions from holograms with stripes

Empty area	25%	50%	75%
PSNR(dB)	24.26	18.16	14.62

the distorted image reconstructed from a hologram with stripes at a pixel (i, j), and the mean square error (MSE) gives the average square of their difference; the parameters I and J give the number of pixels along the x and y axes. The obtained PSNR values are given in Table 2.

The numbers in the "empty area" row give the percentage of the region with zero intensity in the fringe pattern. As can be seen from Table 2, the PSNR value is low even at an empty area of 25%, and further decreases with its increase in the fringe pattern. Obviously, high quality of the reconstructed image can be achieved by reducing the empty area in the fringe pattern.

IV. QUALITY ENHANCEMENT BY ADAPTIVE SLM PARTITIONING

The method we propose for improving color reproduction of a wavefront printer is based on the holographic principle itself. Contrary to the existing mosaic printing, in which each elemental hologram gets a single color, we propose applying the space-division exposure method to the elemental holograms themselves by dividing the SLM area into three subareas to print the RGB colors. In addition, instead of fixing the RGB subareas to be equal to 1/3 of the SLM each, we propose to adapt their sizes L_R, L_G, L_B according to the overall color content in the point clouds attached to the elemental holograms.

Consider a simplified example of a point cloud consisting of 16 red points, 4 green points, and 1 blue point. Obviously the blue channel gives a minor contribution to image quality when playing back the hologram, compared to the red and green channels. The impact of the red channel is the most pronounced. Based on this consideration, a gain in image quality can be achieved if a color channel with higher impact gets more pixels in the SLM, or more space on the holographic plate, than a channel with lower impact. This idea is elucidated in Fig. 7. The ratio between the RGB subareas is adjusted according to their contribution in the overall color content:

$$L_R^{ij} : L_G^{ij} : L_B^{ij} = R^{ij} : G^{ij} : B^{ij}, i = 1, \ldots, K, j = 1, \ldots, L \quad (10)$$

The proposed subdivision is easily implemented by feeding the input data only to the SLM subarea that corresponds to the primary color to be printed. By adapting the recording geometry to the color content, the damage caused by low-intensity or empty color channels is minimized, and undesirable

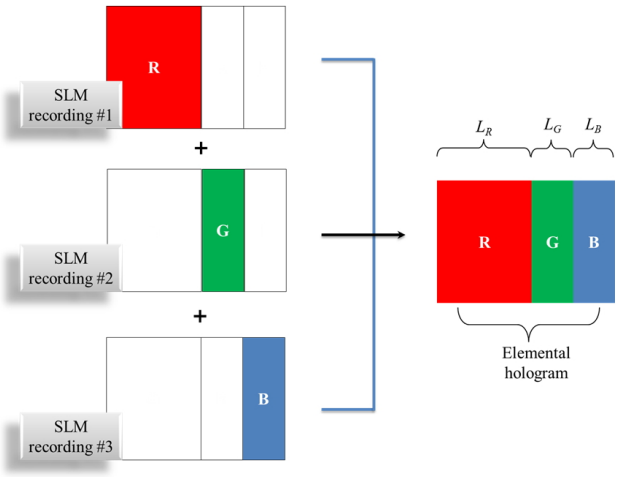

FIG. 7. SLM partitioning with adaptive size of CGH subareas corresponding to primary colors.

artifacts can be avoided. However, adaptive subdivision of the elemental hologram inevitably changes the color expression. Actually, to maintain the color balance given by Eq. (2) in the representation of the 3D object, the hologram should exhibit the ability to reflect the primary colors equally.

Assume that a white-light source such as D65 is used to reconstruct the printed hologram, and that the ratio between the RGB intensities it provides is 1 : 1 : 1. (Technically speaking, this ratio for the D65 source is not 1 : 1 : 1, and perception of colors depends on the sensitivity of the human eye, but further analysis will be postponed for future study.) Then, if the primary colors are recorded as patches of the same size on the holographic emulsion, equal brightness in a reconstruction of RGB colors at a given intensity is achieved by equalizing the diffraction efficiencies for the three wavelengths used in recording. This prevents a particular color from being brighter than the others when playing back the hologram. In general, panchromatic light-sensitive materials exhibit different diffraction efficiencies at the different RGB wavelengths [6]. For better comprehension, Fig. 8 gives a schematic representation of the exposure characteristics for the wavelengths of primary colors that might be observed for a typical light-sensitive material used for holographic printing. The exposure characteristic gives the diffraction efficiency as a function of exposure energy. The curves in Fig. 8 can be plotted also as a function of exposure time, provided the R, G, and B lasers deliver beams with equal intensities in the plane of the hologram. The exposure characteristics allow for determination of the maximum efficiency for each color. Because the maximum diffraction efficiencies E_R, E_G, E_B for the primary colors are different, the RGB recordings should be made with exposure times that guarantee efficiencies equal to the smallest value in the E_R, E_G, E_B set; as a rule, the smallest diffraction efficiency is that for the blue spectral region (Fig. 8). Therefore, to ensure equal reflection ability of the

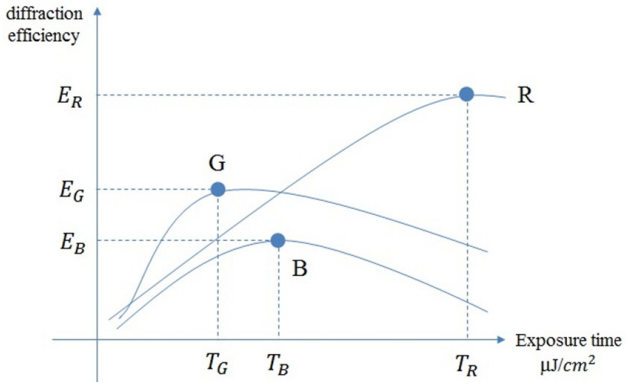

FIG. 8. Schematic representation of exposure characteristics for the RGB wavelengths.

elemental holograms at the RGB wavelengths when the subareas L_R, L_G, L_B are different, one should correspondingly adjust the diffraction efficiencies to become

$$E'_R : E'_G : E'_B \propto \frac{1}{L_R} : \frac{1}{L_G} : \frac{1}{L_B} \tag{11}$$

The change in diffraction efficiency can be achieved by varying the exposure time. In the existing mosaic exposure delivery, the optical header (Fig. 9) of the wavefront printer prints one elemental hologram at a time with one of the three RGB colors, and then moves to the next one. To print the RGB subareas into one elemental hologram, the fringe pattern displayed on the SLM is divided into subpatterns, corresponding to the RGB channels, that are printed with the optical header controlled as shown in Fig. 10. The exposure times are chosen with respect to the exposure characteristics of the used panchromatic holographic emulsion and Eq. (11). Thus, one needs to fulfill the following steps in recording each elemental hologram:

i) Evaluation of the color content for the point cloud corresponding to the elemental hologram, from Eq. (2);
ii) adaptation of the subareas L_R, L_G, L_B on the SLM, according to Eq. (10);
iii) adjustment of exposure times for the primary colors, from Eq. (11), and the exposure characteristics of the holographic emulsion;
iv) successive recordings at the wavelengths of the primary colors; and
v) shift of the X-Y stage to the next elemental hologram.

While the second step in the procedure described above is implemented digitally, and for this reason is very precise, the third step relies on the measured exposure characteristics of the holographic emulsion used, and inevitably provides only approximate values for the RBG exposure times. Nevertheless, the improvement in color reproduction realized by combining numerical and analog estimates, as shown in the next Section, proves the feasibility of the proposed method.

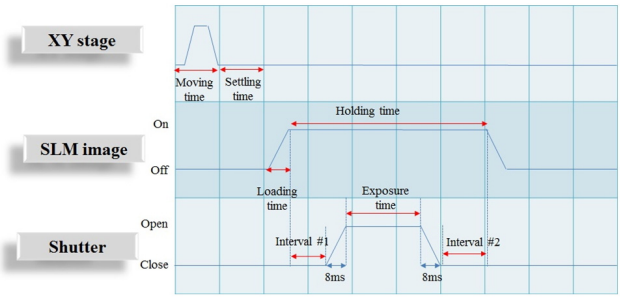

FIG. 9. Time sequence in conventional mosaic recording of an elemental hologram.

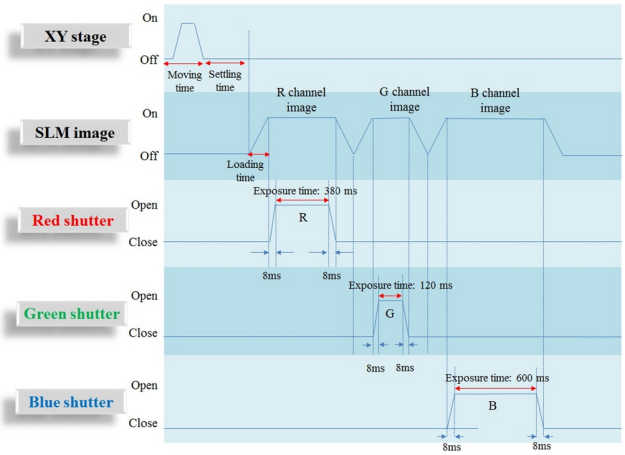

FIG. 10. Time sequence in the recording of an elemental hologram with adaptive SLM partitioning.

V. EXPERIMENTAL CHECK

This study was conducted using the holographic wavefront printer shown in Fig. 11. A photograph of the experimental system is shown in Fig. 12. In the printer's optical system, three DPSS lasers with wavelengths of 473, 532, and 633 nm plus mechanical shutters were used for color production. A polarizing beam splitter (PBS) divided the laser beam in use into reference and object beams. The intensity ratio of the object and reference beams for each of the lasers was adjusted with a half wave plate (HWP). The CGHs to be recorded were displayed on an amplitude-type SLM. The light diffracted from the SLM was collected by the lens L_1 of the telecentric lens system shown in Fig. 2; the spatial filter located at the rear focal plane of this lens cut off the undesired zeroth- and first-order diffracted beams. The -1st -order diffracted beam was demagnified by the lens L_2 with a demagnification factor M = 0.064. The filtered and demagnified beam acted as an object beam for the recording of an elemental volume hologram. For this purpose, a mutually coherent reference beam impinged

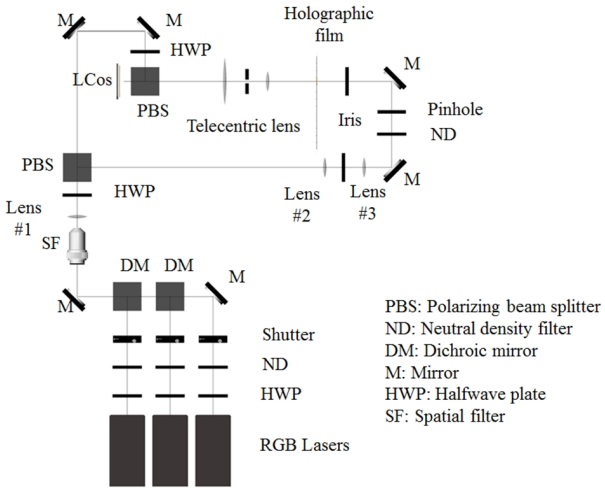

FIG. 11. Schematic of the wavefront printer used in the experiments.

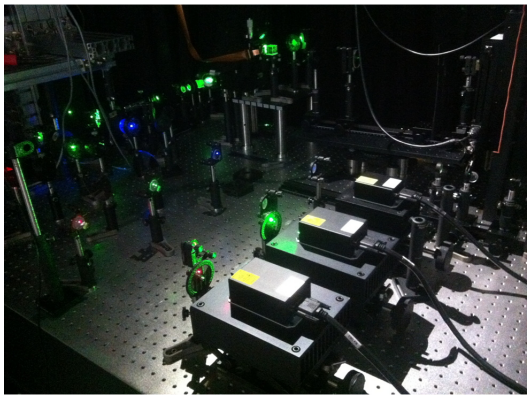

FIG. 12. A photograph of the experimental setup.

FIG. 13. A photograph of the reconstruction from a volume hologram printed with conventional mosaic recording.

FIG. 14. A photograph of the reconstruction from a volume hologram printed with adaptive spatial partitioning of the SLM.

upon the holographic plate on the side opposite the object beam. Printer operation was controlled by computer in the following sequence: (i) shift of the holographic plate to the desired location of the elemental hologram using an X-Y stage; (ii) loading in sequence the RGB fringe patterns onto the SLM; and (iii) successive holographic recording by switching on and off the required laser beam with the corresponding shutter, while controlling the exposure time. We used the extra-fine-grain silver halide emulsion Ultimate08 [24]. During the recording of each color, the reference beam at the corresponding wavelength illuminated the entire elemental hologram. The SLM used was an LCoS, manufactured by Sony, with a pixel pitch of 7 μm and a resolution of 1920 × 1080 pixels; therefore, the maximum size of the printable elemental hologram was 860.16 μm × 483.84 μm. The CGHs were generated as follows: first, a computer-graphic model of the 3D object was composed using a specialized software tool, and then point clouds for the object were extracted using graphics software, such as OpenGL. Last, the final CGH files were obtained by the fast phase-added algorithm described in Sec. 4. Photographs of reconstructions from holograms printed by the conventional mosaic method and by adaptive SLM partitioning are shown in Figs. 13 and 14 respectively. To verify the concept of the proposed method, we chose an object with unbalanced color content, from which blue was practically absent. The stripe structure superimposed on the reconstructed image is so strongly pronounced in the first case (Fig. 13) that the obtained result is completely unacceptable. In contrast, the result obtained by adaptive SLM partitioning and adjusting the exposure time for each of the primary colors (Fig. 14) presents smooth, bright color surfaces.

VI. CONCLUSION

This paper presents a method to improve color reproduction in a wavefront printer using spatial division of exposures in primary colors. The wavefront printer records a volume reflection hologram as a 2D array of elemental holograms from CGHs displayed on an SLM. The wavefront coming from the object is extracted by filtering in the spatial-fre-

quency domain. Mosaic delivery of exposures, in which an elemental hologram receives only a single color, avoids crosstalk between the color channels and provides bright reconstruction with saturated colors. It may, however, cause undesirable artifacts superimposed on the reconstructed image, if a color channel is empty or carries a very low-intensity fringe pattern. To solve this issue, we propose adaptive partitioning of the SLM according to the color content encoded in the input CGHs, and combined it with a controllable change of exposure times for the recording of primary colors, to maintain color balance when reconstructing the object. The CGH for a given elemental hologram is computed by ray-casting, which determines a set of primitives (points or polygons) to represent the 3D object. Replacing a single exposure of an elemental hologram with three exposures in primary colors increases only slightly the total printing time for printers with CW lasers, in view of the fact that the settling time of the X-Y stage is much longer than the exposure time. The method is verified using a color wavefront printer with demagnification of the object beam. The CGHs to be fed to the SLM were generated from a set of point clouds using a fast phase-added approach. The quality of reconstruction achieved with the proposed method demonstrates its efficiency in eliminating the stripe artifacts that are superimposed on reconstructed images in conventional mosaic recording.

ACKNOWLEDGMENT

This work was supported by the IT R&D program of MSIP/Giga KOREA [GK14D0100, Development of Telecommunications Terminal with Digital Holographic Table-top Display].

REFERENCES

1. D. Gabor, "A new microscopic principle," Nature **161**, 777-778 (1948).
2. E. Leith and J. Upatnieks, "Reconstructed wavefronts and communication theory," J. Opt. Soc. Am. **52**, 1123-1128 (1962).
3. Y. N. Denisyuk, "On the reflection of optical properties of an object in the wave field of light scattered by it," Doklady Akademii Nauk SSSR **144**, 1275-1278 (1962).
4. L. Onural, F. Yaras, and H. Kang, "Digital holographic three-dimensional video displays," Proc. IEEE **99**, 576-589 (2011).
5. H. Kang, E. Stoykova, J. Park, S. Hong, and Y. Kim, "Holographic printing of white-light viewable holograms and stereograms," in *Holography - Basic Principles and Contemporary Applications*, E. Mihaylova ed. (InTech, 2013).
6. H. Bjelkhagen and D. Brotherton-Ratcliffe, *Ultra-realistic Imaging – Advanced Techniques in Analogue and Digital Color Holography* (Taylor and Francis, 2013).
7. M. Yamaguchi, N. Ohyama, and T. Honda, "Holographic three-dimensional printer: New method," Appl. Opt. **31**, 217-222 (1992).
8. D. Brotherton-Ratcliffe, S. Zacharovas, R. Bakanas, J. Pileckas, A. Nikolskij, and J. Kuchin, "Digital holographic printing using pulsed RGB lasers," Opt. Eng. **50**, 091307 (2011).
9. H. Yoshikawa and M. Tachinami, "Development of direct fringe printer for computer-generated holograms," Proc. SPIE **5742**, 02777-786X (2005).
10. T. Yamaguchi, O. Miyamoto, and H. Yoshikawa, "Volume hologram printer to record the wavefront of three-dimensional objects," Opt. Eng. **51**, 075802 (2012).
11. H. Kang and E. Stoykova, "Wave-field recording onto a holographic emulsion," in *Proc. Second Korea-Japan Workshop on Digital Holography and Information Photonics* (Tokushima, Japan, 19-21 Nov. 2012), http://dhip.i-photonics.jp
12. H. Kang, S. Hong, Y. Kim, E. Stoykova, K.-M. Jung, and K.-H. Seo, "Holographic printer for filtering holographic fringe pattern and recording that on holographic recording medium by the hogel and holographic printing method thereof," KR Patent 1014231630000 (2014).
13. H. Kang, E. Stoykova, H. Yoshikawa, S. Hong, and Y. Kim, "Comparison of system properties for wavefront holographic printers," in *Fringe 2013* (Springer-Verlag, Berlin-Heidelberg, 2014), pp. 855-858.
14. W. Nishii and K. Matsuashima, "A wavefront printer using phase-only spatial light modulator for producing computer-generated volume holograms," Proc. SPIE **9006**, 90061F (2014).
15. M. Yamaguchi, T. Honda, N. Ohyama, and J. Ishikawa, "Multidot recording of rainbow and multicolor holographic stereograms," Opt. Commun. **110**, 523-528 (1994).
16. S. Maruyama, Y. Ono, and M. Yamaguchi, "High-density recording of full color full parallax holographic stereogram," Proc. SPIE **6912**, 69120N (2008).
17. F. Yang, Y. Murakami, and M. Yamaguchi, "Digital color management in full-color holographic three-dimensional printer," Appl. Opt. **51**, 4343-4352 (2012).
18. H. Bjelkhagen and E. Mirlis, "Color holography to produce highly realistic three-dimensional images," Appl. Opt. **47**, A123-A133 (2008).
19. H. Zhang, N. Collings, J. Chen, B. Crossland, D. Chu, and J. Xie, "Full parallax three-dimensional display with occlusion effect using computer generated hologram," Opt. Eng. **50**, 074003 (2011).
20. T. Ichikawa, K. Yamaguchi, and Y. Sakamoto, "Realistic expression for full-parallax computer-generated holograms with the ray tracing method," Appl. Opt. **52**, A201-A209 (2013).
21. H. Kim, J. Hahn, and B. Lee, "Mathematical modeling of triangle-mesh-modeled three-dimensional surface objects for digital holography," Appl. Opt. **47**, D117-D127 (2008).
22. H. Kang, T. Yamaguchi, H. Yoshikawa, S. C. Kim, and E. S. Kim, "Acceleration method of computing a compensated phase-added stereogram on a graphic processing unit," Appl. Opt. **47**, 5784-5789 (2008).
23. H. Kang, T. Yamaguchi, and H. Yoshikawa, "Accurate phase-added stereogram to improve the coherent stereogram," Appl. Opt. **47**, D44-D54 (2008).
24. Y. Gentet and P. Gentet, "Ultimate emulsion and its applications: A laboratory-made silver halide emulsion of optimized quality for monochromatic pulsed and full-color holography," Proc. SPIE **4149**, 56-62 (2000).